AMMRC TR 77-21

AD

RESIDUAL STRESSES IN AN ANISOTROPIC THICK HOLLOW CYLINDER OF CHEMICALLY VAPOR-DEPOSITED MATERIAL DUE TO UNIFORM COOL-DOWN

FRANCIS I. BARATTA
MECHANICS OF MATERIALS DIVISION

October 1977

Approved for public release; distribution unlimited.

ARMY MATERIALS AND MECHANICS RESEARCH CENTER
Watertown, Massachusetts 02172

The findings in this report are not to be construed as an official Department of the Army position, unless so designated by other authorized documents.

Mention of any trade names or manufacturers in this report shall not be construed as advertising nor as an official indorsement or approval of such products or companies by the United States Government.

DISPOSITION INSTRUCTIONS

Destroy this report when it is no longer needed.
Do not return it to the originator.

UNCLASSIFIED

SECURITY CLASSIFICATION OF THIS PAGE (When Data Entered)

REPORT DOCUMENTATION PAGE

READ INSTRUCTIONS BEFORE COMPLETING FORM

1. REPORT NUMBER: AMMRC-TR-77-21	2. GOVT ACCESSION NO.
3. RECIPIENT'S CATALOG NUMBER	
4. TITLE (and Subtitle): RESIDUAL STRESSES IN AN ANISOTROPIC THICK HOLLOW CYLINDER OF CHEMICALLY VAPOR-DEPOSITED MATERIAL DUE TO UNIFORM COOL-DOWN	5. TYPE OF REPORT & PERIOD COVERED: Final Report
	6. PERFORMING ORG. REPORT NUMBER
7. AUTHOR(s): Francis I. Baratta	8. CONTRACT OR GRANT NUMBER(s)
9. PERFORMING ORGANIZATION NAME AND ADDRESS: Army Materials and Mechanics Research Center, Watertown, Massachusetts 02172, DRXMR-TM	10. PROGRAM ELEMENT, PROJECT, TASK AREA & WORK UNIT NUMBERS: D/A Project: 1T161101A91A, AMCMS Code: 611101.91A0011, Agency Accession: DA OF4769
11. CONTROLLING OFFICE NAME AND ADDRESS: U. S. Army Materiel Development and Readiness Command, Alexandria, Virginia 22333	12. REPORT DATE: Oct 77
	13. NUMBER OF PAGES: 26
14. MONITORING AGENCY NAME & ADDRESS (if different from Controlling Office): 28p.	15. SECURITY CLASS. (of this report): Unclassified
	15a. DECLASSIFICATION/DOWNGRADING SCHEDULE

16. DISTRIBUTION STATEMENT (of this Report)

Approved for public release; distribution unlimited.

17. DISTRIBUTION STATEMENT (of the abstract entered in Block 20, if different from Report)

18. SUPPLEMENTARY NOTES

19. KEY WORDS (Continue on reverse side if necessary and identify by block number)

Residual stress
Vapor deposition
Anisotropy

20. ABSTRACT (Continue on reverse side if necessary and identify by block number)

(SEE REVERSE SIDE)

Block No. 20

alpha

ABSTRACT

Residual stresses are derived for a transversely anisotropic thick hollow cylinder which has been chemically vapor deposited at an elevated temperature. Such stresses arise because of the differential rates of contraction in the radial and tangential directions and the anisotropic elastic constants. Residual stress distributions for cylinders with a wall ratio (outer to inner radius) of 1.30 of pyrolytic graphite and pyrolytic silicon carbide (α-SiC) are presented as a function of the radius to inner radius. The effect of the variation of the elastic anisotropy on the tangential stress at the inner and outer radii is presented as a function of the wall ratio. Finally, the tangential and axial stresses at the inner and outer radii and the maximum radial stress of chemically vapor-deposited α-SiC are presented as a function of the wall ratio.

NOMENCLATURE

a	inner radius of cylinder
b	outer radius of cylinder
c_{qr}	elastic stiffnesses, i.e., c_{11}, c_{12}, c_{13}, c_{14}, c_{33}, c_{44} (see Appendix C)
m	anisotropy parameter
r	radius coordinate
s_{qr}	elastic compliances, i.e., s_{11}, s_{12}, s_{13}, s_{14}, s_{33}, s_{44} (see Appendix C)
t	thickness of thin-walled cylinder
u	displacement in the radial direction
W	wall ratio = b/a
z	axial coordinate
$E_{\theta\theta}$	Young's modulus in the θ direction
E_{rr}	Young's modulus in the r direction
$E_{zz} = E_{\theta\theta}$	Young's modulus in the z and θ directions
T_a	ambient temperature
T_d	deposition temperature
$\beta_{\theta\theta}$	contractual strain in the θ direction due to cool-down
β_{rr}	contractual strain in the r direction due to cool-down
$\varepsilon_{\theta\theta} = u/r$	strain in θ direction
$\varepsilon_{rr} = du/dr$	strain in the r direction
ε_{zz}	strain in z direction
θ	angular coordinate
$\nu_{z\theta} = \nu_{\theta\theta}$	Poisson's ratio in the θ direction due to a stress in z direction
$\nu_{\theta z} = \nu_{\theta\theta}$	Poisson's ratio in the z direction due to a stress in θ direction
$\nu_{\theta r}$	Poisson's ratio in the r direction due to a stress in the θ direction
$\nu_{r\theta}$	Poisson's ratio in the θ direction due to a stress in the r direction
ν_{zr}	Poisson's ratio in the r direction due to a stress in the z direction
ν_{rz}	Poisson's ratio in the z direction due to a stress in the r direction
$\sigma_{\theta\theta}$	stress in the θ direction (tangential stress)
σ_{rr}	stress in the r direction (radial stress)
σ_{zz}	stress in the z direction (axial stress)
$\sigma_{\theta\theta}/C$	tangential stress ratio

CONTENTS

I. INTRODUCTION

Silicon carbide (SiC) and silicon nitride (Si_3N_4) are candidate materials for high temperature applications in ceramic gas turbine for vehicles[1] and electric power generation.[2] The usual method of manufacturing these materials into intricate shapes is by hot pressing billets and diamond grinding. Such a finishing process is difficult and expensive because of the high hardness of these materials. Alternative methods of manufacturing silicon carbide and silicon nitride have been investigated to reduce fabrication costs. One of these methods that appears to have potential promise is the chemical vapor deposition (CVD) process, because it readily allows the formation of complex shapes of ceramic materials on preshaped substrates. This, of course, minimizes mechanical fabrication procedures.

Vapor deposition is the formation of a solid deposit occurring as condensation of elements or compounds from the vapor state. Chemically vapored deposits are formed by chemical reactions which take place on, at, or near the deposition surface, i.e., mandrel or substrate. Deposition temperatures of structural materials of interest are relatively high; for example, pyrolytic silicon carbide can be formed at temperatures as high as 1800 C (3272 F) and pyrolytic silicon nitride up to 1500 C (2732 F). The usual method of producing pyrolytic shapes of silicon carbide and silicon nitride is to introduce the appropriate gas mixture into a chamber containing the heated mandrel, allow evacuation of the exhaust gases, and with proper control of the complex physical and chemical steps, deposition will occur. For a detailed description of the CVD silicon carbide process see, for example, Weiss[3] and for the CVD silicon nitride process see Niihara.[4]

Although CVD silicon carbide or silicon nitride shapes are relatively easy to produce, their tensile strengths are less than that of respective hot-pressed materials. This, in part, is due to residual stresses inherent in the process of producing vapor-deposited materials which arise because of several possible mechanisms.[3,5] Even though physical processes such as temperature gradient and structural growth or phase changes during deposition may be mathematically tractable, the only mechanism considered here resulting in residual stress is that caused by the thermal anisotropic coefficients of expansion during uniform cool-down.

The complete detailed derivation for the thick-walled cylinder case is given in Appendix A. A thick hollow cylinder configuration was chosen as the geometry to analyze because such a configuration is compatible with cylindrical anisotropy and also provides an ideal vehicle by which the residual strains and thus the

1. McLEAN, A. F. *Ceramics in Small Vehicular Gas Turbines* in Ceramics for High Performance Applications. Proc of the 2nd Army Materials Technology Conf., ed. by J. J. Burke, A. E. Gorum, and R. N. Katz, Brook Hill Publ. Co., 1974, p. 9-36.
2. BRATTON, R. J. *Ceramics in Gas Turbines for Electrical Power Generation* in Ceramics for High Performance Applications. Proc. of the 2nd Army Materials Technology Conf., ed. by J. J. Burke, A. E. Gorum, and R. N. Katz, Brook Hill Publ. Co., 1974, p. 37-60.
3. WEISS, J. *The Relationship of Structure and Properties to Deposition Conditions and the Origin of Residual Stress in Chemically Vapor Deposited Silicon Carbide.* Ph.D. Thesis, Rensselaer Polytechnic Inst., 1974, p. 49-53.
4. NIIHARA, K., and HIRAI, T. *Chemical Vapor-Deposited Silicon Nitride.* J. of Mater. Sci., v. 11, 1976, p. 593-603.
5. POWELL, C. F., OXLEY, J. H., and BLOCHER, J. M., Jr. *Vapor Deposition.* John Wiley and Sons, Inc., 1966, p. 659-662.

stresses can be experimentally determined.* The resulting formulae are reduced so that they are applicable to a thin-walled cylinder and these equations are given in Appendix B.

In order to provide numerical results, two materials were considered: pyrolytic graphite and pyrolytic silicon carbide. Pyrolytic graphite was developed and exploited for use in missiles during the early 1960's. Its properties are well characterized and are given in Appendix C. Calculations resulting from such well-defined properties will reflect the accuracy of the data base. However, there is a paucity of experimental pyrolytic silicon carbide (α-SiC) property data as indicated in Appendix C, and idealized values of the anisotropic elastic constants were used in determining the distribution and magnitudes of the residual stresses. Therefore, the residual stress calculations are those that would result when the material (α-SiC) has high preferential orientation occurring at a deposition temperature of 1800 C (3272 F) and thus these values are considered as upper bounds.

As previously mentioned, the detailed steps of mathematical analysis is given in Appendix A and will not be repeated here. However, a brief description of the physical problem and analysis is given below, as well as resulting pertinent equations.

II. ANALYSIS

The geometry considered is an infinitely long, thick hollow cylinder with an inner radius a and outer radius b. A cylindrical coordinate system is used with the three normal directions θ, r, and z, as shown in Figure 1. It is assumed that the material, deposited at the elevated temperature, is preferentially aligned in the radial direction. Thus, there is cylindrical anisotropy. It is assumed that elastic parameters remain constant during deposition and subsequent uniform cool-down and there is no mechanical interaction between the substrate (mandrel) and deposit, i.e., no adhesion and/or no expansion coefficient mismatch. Such problems can be handled independently, see Reference 6 for example. Also, during deposition the temperature throughout the body is constant and uniform.

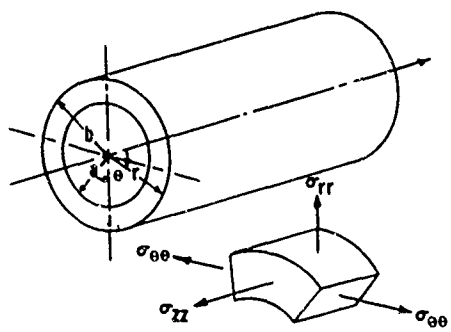

Figure 1. Cylindrical coordinate system.

*As of this writing no experimental results have been obtained.

6. RUDDLESEN, S. N. *Thermal Stresses in Pyrolytic Deposits* in Special Ceramics 4, ed. by P. Popper, British Ceramic Research Assoc., 1968, p. 153-163.

The analysis given in Appendix A consists of formulating the stress-strain relationships of a body with cylindrical anisotropy and substituting the relationships for the two stresses $\sigma_{\theta\theta}$ and σ_{rr} into the governing equilibrium equation. This results, after some manipulation, in the formulation of an equidimensional Euler or Cauchy[7] second-order linear differential equation. This differential equation is then solved to yield radial displacement u as a function of the radius r. Finally, through the use of the stress-strain relationships and the boundary conditions the stresses $\sigma_{\theta\theta}$, σ_{rr}, and σ_{zz} are derived. The equations for these stresses are given in the following:

$$\sigma_{\theta\theta} = \left(\frac{C}{1-m^2}\right)\left\{1 + \left(\frac{m}{1-W^{2m}}\right)\left[(W^{m+1}-1)(r/a)^{m-1} - (W^{m-1}-1)\frac{W^{m+1}}{(r/a)^{m+1}}\right]\right\} \tag{1}$$

$$\sigma_{rr} = \left(\frac{C}{1-m^2}\right)\left\{1 + \left(\frac{m}{1-W^{2m}}\right)\left[(W^{m+1}-1)(r/a)^{m-1} + (W^{m-1}-1)\frac{W^{m+1}}{(r/a)^{m+1}}\right]\right\} \tag{2}$$

and

$$\sigma_{zz} = \frac{C}{(1-m^2)(1-W^{2m})}\left\{(\nu_{\theta r} + m\nu_{\theta\theta})(W^{m+1}-1)\left[(r/a)^{m-1} - \left(\frac{2}{1+m}\right)\frac{(W^{m+1}-1)}{(W^2-1)}\right]\right.$$

$$\left. + (\nu_{\theta r} - m\nu_{\theta\theta})(W^{m-1}-1)\,W^{m+1}\left[\frac{1}{(r/a)^{m+1}} - \left(\frac{2}{1-m}\right)\frac{(W^{1-m}-1)}{(W^2-1)}\right]\right\} \tag{3}$$

where

$$C = \frac{[\beta_{rr} - (1+\nu_{\theta\theta} - \nu_{\theta r})\beta_{\theta\theta}]E_{\theta\theta}}{\left(1 - \nu_{\theta\theta}^2\right)} \qquad \text{and}$$

$$m = \left[E_{\theta\theta}/E_{rr}\left(\frac{1-\nu_{\theta r}\nu_{r\theta}}{1-\nu_{\theta\theta}^2}\right)\right]^{1/2}$$

7. HILDEBRAND, F. B. *Advanced Calculus for Applications.* Prentice-Hall, 1962, p. 13.

The tangential, radial, and axial strains are given by the following formulas:

$$\varepsilon_{\theta\theta} = \frac{u}{r} = \frac{C[(1-\nu_{\theta\theta})E_{\theta\theta}/E_{rr} - 2\nu_{\theta r}^2]}{E_{\theta\theta}(1-m^2)(1-W^{2m})} \left\{ \frac{(W^{m+1}-1)}{[\nu_{\theta r}+m(1-\nu_{\theta\theta})]} (r/a)^{m-1} \right.$$

$$\left. + \frac{(W^{m-1}-1)}{[\nu_{\theta r}- m(1-\nu_{\theta\theta})]} \frac{W^{m+1}}{(r/a)^{m+1}} \right\} + \frac{a_1}{1-m^2} \tag{4}$$

$$\varepsilon_{rr} = \frac{du}{dr} = \frac{mC[(1-\nu_{\theta\theta})E_{\theta\theta}/E_{rr}- 2\nu_{\theta r}^2]}{E_{\theta\theta}(1-m^2)(1-W^{2m})} \left\{ \frac{(W^{m+1}- 1)}{[\nu_{\theta\theta}+ m(1-\nu_{\theta\theta})]} (r/a)^{m-1} \right.$$

$$\left. - \frac{(W^{m-1}- 1)}{[\nu_{\theta\theta}- m(1-\nu_{\theta\theta})]} \frac{W^{m+1}}{(r/a)^{m+1}} \right\} + \frac{a_1}{1-m^2} \tag{5}$$

and

$$\varepsilon_{zz} = \beta_{\theta\theta} - \frac{C(\nu_{\theta\theta}+\nu_{\theta r})}{E_{\theta\theta}(1-m^2)} - \frac{2C}{E_{\theta\theta}(1-m^2)(1-W^{2m})(W^2- 1)} \left[\frac{(\nu_{\theta\theta}+m\nu_{\theta\theta})}{1+m} (W^{m+1}- 1)^2 \right.$$

$$\left. + \frac{(\nu_{\theta r}- m\nu_{\theta\theta})}{1-m} (W^{m-1}-1)(W^{1-m}-1)W^{m+1} \right] \tag{6}$$

where

$$a_1 = \left(\frac{1}{1-\nu_{\theta\theta}}\right) \left[(1-\nu_{\theta\theta}-\nu_{\theta r})\beta_{rr} - (1-2\nu_{r\theta})\left(\frac{E_{\theta\theta}}{E_{rr}}\right)\beta_{\theta\theta} \right]$$

The stresses $\sigma_{\theta\theta}$ and σ_{zz} at r = a and r = b were also determined and are:

$$(\sigma_{\theta\theta})_{r=a} = \left(\frac{C}{1-m^2}\right) \left\{ 1 + \left(\frac{m}{1-W^{2m}}\right) [2W^{m+1} - 1 - W^{2m}] \right\} \tag{7}$$

$$(\sigma_{\theta\theta})_{r=b} = \left(\frac{C}{1-m^2}\right) \left\{ 1 - \left(\frac{m}{1-W^{2m}}\right) [2W^{m-1}- 1 - W^{2m}] \right\} \tag{8}$$

$$(\sigma_{zz})_{r=a} = \frac{C}{(1-m^2)(1-W^{2m})} \left\{(\nu_{\theta r}+m\nu_{\theta\theta})(W^{m+1}-1)\left[1 - (\frac{2}{1+m})\frac{(W^{m+1}-1)}{(W^2-1)}\right]\right.$$

$$\left. + (\nu_{\theta r}-m\nu_{\theta\theta})(W^{m-1}-1)W^{m+1}\left[1 - (\frac{2}{1-m})\frac{(W^{1-m}-1)}{(W^2-1)}\right]\right\} \quad (9)$$

and

$$(\sigma_{zz})_{r=b} = \frac{C}{(1-m^2)(1-W^{2m})} \left\{(\nu_{\theta r}+m\nu_{\theta\theta})(W^{m+1}-1)\left[W^{m-1} - \left(\frac{2}{1+m}\right)\frac{(W^{m+1}-1)}{(W^2-1)}\right]\right.$$

$$\left. + (\nu_{\theta r}-m\nu_{\theta\theta})(W^{m-1}-1)\left[1-\left(\frac{2}{1-m}\right)\left(\frac{W^{1-m}-1}{W^2-1}\right)W^{m+1}\right]\right\} \quad (10)$$

From inspection it was determined that the absolute value of maximum tangential and axial stress occurs at r = a. Also, the absolute maximum radial stress was obtained by maximizing Equation 2 and found to be located at:

$$r/a = \left[\left(\frac{m+1}{m-1}\right)\frac{(W^{m-1}-1)W^{m+1}}{(W^{m+1}-1)}\right]^{1/2m} \quad (11)$$

The tangential and radial strains at the inner and outer radii can also be obtained and are:

$$(\varepsilon_{\theta\theta})_{r=a} = \frac{C[(1-\nu_{\theta\theta})E_{\theta\theta}/E_{rr}-2\nu_{\theta r}^2]}{E_{\theta\theta}(1-m^2)(1-W^{2m})}\left\{\frac{(W^{m+1}-1)}{\nu_{\theta r}+(1-\nu_{\theta\theta})m} + \frac{(W^{m-1}-1)W^{m+1}}{\nu_{\theta r}-(1-\nu_{\theta\theta})m}\right\} + \frac{a_1}{1-m^2} \quad (12)$$

$$(\varepsilon_{\theta\theta})_{r=b} = \frac{C[(1-\nu_{\theta\theta})E_{\theta\theta}/E_{rr}-2\nu_{\theta r}^2]}{E_{\theta\theta}(1-m^2)(1-W^{2m})}\left\{\frac{(W^{m+1}-1)W^{m-1}}{\nu_{\theta\theta}+(1-\nu_{\theta\theta})m} + \frac{(W^{m-1}-1)}{\nu_{\theta r}-(1-\nu_{\theta\theta})m}\right\} + \frac{a_1}{1-m^2} \quad (13)$$

$$(\varepsilon_{rr})_{r=a} = \frac{mC[(1-\nu_{\theta\theta})E_{\theta\theta}/E_{rr} - 2\nu_{\theta r}^2]}{E_{\theta\theta}(1-m^2)(1-W^{2m})}\left\{\frac{(W^{m+1}-1)W^{m-1}}{\nu_{\theta r} + (1-\nu_{\theta\theta})m} - \frac{(W^{m-1}-1)W^{m+1}}{\nu_{\theta r}-(1-\nu_{\theta\theta})m}\right\}$$

$$+ \frac{a_1}{1-m^2} \quad (14)$$

and

$$(\varepsilon_{1r})_{r=b} = \frac{mC\left[(1-\nu_{\theta\theta})E_{\theta\theta}/E_{rr} - 2\nu_{\theta r}^2\right]}{E_{\theta\theta}(1-m^2)(1-W^{2m})}\left\{\frac{(W^{m+1}-1)W^{m-1}}{\nu_{\theta r}+(1-\nu_{\theta\theta})m} - \frac{(W^{m-1}-1)}{\nu_{\theta r}-(1-\nu_{\theta\theta})m}\right\} + \frac{a_1}{1-m^2} \tag{15}$$

In Appendix B the formulae describing residual tangential and axial stresses at the inner and outer radii can be reduced to those of thin-wall cylinder theory. Their usage is dependent upon the error one is willing to tolerate and that error is dependent on the wall ratio and the material, in particular, the value of m. Refer to Section IV for a detailed discussion of this. However, for the sake of completeness these equations are given by the following:

$$(\sigma_{\theta\theta})_{r=\begin{cases}a\\b\end{cases}} = \pm \frac{C\ t/a}{2+(2m-1)t/a} \tag{16}$$

and

$$(\sigma_{zz})_{r=\begin{cases}a\\b\end{cases}} = \pm \frac{\nu_{\theta\theta}C\ t/a}{2(1+m\ t/a)} \tag{17}$$

In the next section both the more exact equations and the thin-wall theory equations are applied to examples of cylinders of two different materials having a wall ratio of 1.30 and a great difference in anisotropic elastic constants. The tangential stress ratio $\sigma_{\theta\theta}/C$ at the inner and outer radii is evaluated as a function of the wall ratio and for a wide range of the anisotropy parameter m. Finally, the residual tangential and axial stress at the inner and outer radii as well as the maximum residual radial stress is determined for α-SiC as a function of the wall ratio.

III. RESULTS AND DISCUSSION

The material properties of two transversely anisotropic materials, pyrolytic graphite and pyrolytic silicon carbide, were utilized to demonstrate the applicability of the pertinent equations. Pyrolytic graphite was chosen because its properties are well documented.[5,8,9] Pyrolytic silicon carbide was chosen because of its attractive potential use as a high temperature structural material. In Reference 10, it is indicated that the anisotropic elastic constants associated with the hexagonal silicon carbide system (α-SiC 6H) are not likely to be different from other polytypes. Not all of the stiffnesses for α-SiC 6H, which were determined experimentally in Reference 10, were obtained, whereas all of those

8 DONADIO, R. N., and PAPPAS, J. *Mechanical Properties of Pyrolytic Graphite* Raytheon Technical Memorandum 1547, 1964

9. High Temperature Materials Inc., Data Sheet, October 1969.

10. ARLT, G., and SCHODDER, G. V. *Some Elastic Constants of Silicon Carbide* J. Acoust. Soc. of Am., v. 37, no. 2, February 1965, p. 384-386

for the trigonal system, which were calculated from idealized consideration, were given and compared closely to those that were experimentally determined for α-SiC 6H. The compliances for the trigonal system were computed via the use of interconversion equations given in Reference 11 and thus the anisotropic elastic constants for a trigonal rather than hexagonal silicon carbide system were utilized in subsequent residual stress determinations.

The coefficients of expansion for hexagonal silicon carbide (α-SiC) were obtained from Reference 12 and are also used in subsequent calculations. The details of how the constants were obtained are given in Appendix C. Anisotropic elastic constants and other constants such as $\beta_{\theta\theta}$, β_{rr}, and m used in residual stress calculations for pyrolytic graphite and pyrolytic silicon carbide are given in Table 1, as well as the reference source, where applicable.

It was intended to examine pyrolytic silicon nitride as well. However, a search of the literature indicated that there were no anisotropic elastic constant data available.

The stress distributions for $\sigma_{\theta\theta}$, σ_{rr}, and σ_{zz}, according to Equations 1 to 3, as a function of r/a and a wall ratio of 1.3 for both pyrolytic graphite and pyrolytic silicon carbide are shown in Figure 2. Although pyrolytic graphite cannot withstand such high self-imposed stresses and would fracture at a much smaller wall ratio, the results are presented to compare the behavior of the two materials.

Table 1. ANISOTROPIC ELASTIC CONSTANTS

Constant	Pyrolytic Graphite	Ref.	Pyrolytic Silicon Carbide	Ref.
$E_{\theta\theta}$	4.29 x 10^6 psi (29.58 x 10^6 MN/m^2)	8	60.6 x 10^6 psi (417.82 x 10^6 MN/m^2)	*
E_{rr}	1.55 x 10^6 psi (10.69 x 10^6 MN/m^2)	8	74.1 x 10^6 psi (510.9 x 10^6 MN/m^2)	*
$\nu_{\theta\theta}$	-0.15	8	+0.255	*
$\nu_{\theta r}$	+0.90	8	+0.079	*
$\nu_{r\theta}$	+0.325	†	+0.097	†
$\beta_{\theta\theta}$	-4600 x 10^{-6} in./in. T_d of 2150 C (3902 F)	9	-9624 x 10^{-6} in./in. T_d of 1800 C (3298 F)	12
β_{rr}	-51,700 x 10^{-6} in./in. T_d of 2150 C (3902 F)	9	-9204 x 10^{-6} in./in. T_d of 1800 C (3298 F)	12
m	1.415	‡	0.932	‡

*Indirectly obtained from Reference 10
†Calculated from the reciprocal relationship $\nu_{r\theta} = \nu_{\theta r} E_{rr}/E_{\theta\theta}$
‡$m = [E_{\theta\theta}/E_{rr}(1-\nu_{\theta r}\nu_{r\theta}/1-\nu_{\theta\theta}^2)]^{\frac{1}{2}}$

11 HEARMON R F S *An Introduction to Applied Anisotropic Elasticity* Oxford U Press, 1961, p 25
12 TAYLOR A and JONES R M *The Crystal Structure and Thermal Expansion of Cubic and Hexagonal Silicon Carbide* Proc of the Conf on Silicon Carbide Pergamon Press 1960 p 147-154

It is not to be inferred here that the stress distributions shown in Figure 2 are absolute. That is, mechanisms such as temperature gradient, phase transformations, for example, will impose other residual stress patterns. The residual stress distributions presented here are caused by only one of the various acting mechanisms and are a part of the sum total.

Notice that $\sigma_{\theta\theta}$ and σ_{rr} as a function of r/a shown in Figure 2a are of opposite sign compared to the corresponding stresses in Figure 2b. This is caused by the constant C, recalling that

$$C = \frac{[\beta_{rr}-(1+\nu_{\theta\theta}-\nu_{\theta r})\beta_{\theta\theta}]E_{\theta\theta}}{1-\nu_{\theta\theta}^2} .$$

The different sign of the tangential and radial stresses for the two materials is due to the relative magnitudes of the radial and tangential shrinkage during cooling. That is, if $\beta_{rr} < (1+\nu_{\theta\theta}-\nu_{\theta r})\beta_{\theta\theta}$ which is typical of pyrolytic graphite, and if $\beta_{rr} > (1+\nu_{\theta\theta}-\nu_{\theta r})\beta_{\theta\theta}$ which was determined for pyrolytic silicon carbide, then the tangential and radial stress distributions will be of opposite sign. The axial stress distributions for the two materials are of the same sign because $\nu_{\theta\theta}$ of the two materials is of opposite sign, thus compensating for opposing sign of the constant C associated with each material.

The absolute values of the stress magnitudes for pyrolytic graphite are greater than those of pyrolytic silicon carbide for the same wall ratio. This is mainly attributed to the constant C, which for pyrolytic graphite is very much greater than that for pyrolytic silicon carbide. Again, the magnitude of C is strongly dependent upon the contraction rates during cooling, i.e., β_{rr} and $\beta_{\theta\theta}$, as well as $E_{\theta\theta}$. Since β_{rr} for pyrolytic graphite is much greater than that of pyrolytic silicon carbide, then pyrolytic graphite will have greater stress magnitudes even though $E_{\theta\theta}$ is an order of magnitude less than that of pyrolytic silicon carbide.

It is interesting to note than even if $\beta_{rr} = \beta_{\theta\theta}$, residual stresses would still persist because of the elastic anisotropy.

The influence of the elastic anisotropy parameter m on the tangential stress at the inner and outer radii of a thick cylinder, Equations 7 and 8, was evaluated as a function of the wall ratio W and is shown by solid curves in Figure 3. Practical values of m ranging from approximately 0.8 to 1.6 for hexagonal and trigonal crystal structures were obtained from References 11 and 13. Therefore, m was varied from 0.50 to 2.0 as shown in Figure 3. Note that beyond a wall ratio of approximately 1.30 the absolute magnitude of the tangential stress ratio increases as m decreases. At wall ratios of approximately less than 1.30 the magnitude of m appears to have little effect on the tangential stress at the inner and outer radii.

13 HEARMON, R F S *The Elastic Constants of Anisotropic Materials - II* Advances in Physics - A Quarterly Supplement of the Phil. Mag., v 5, no 19, July 1956, p. 323-381.

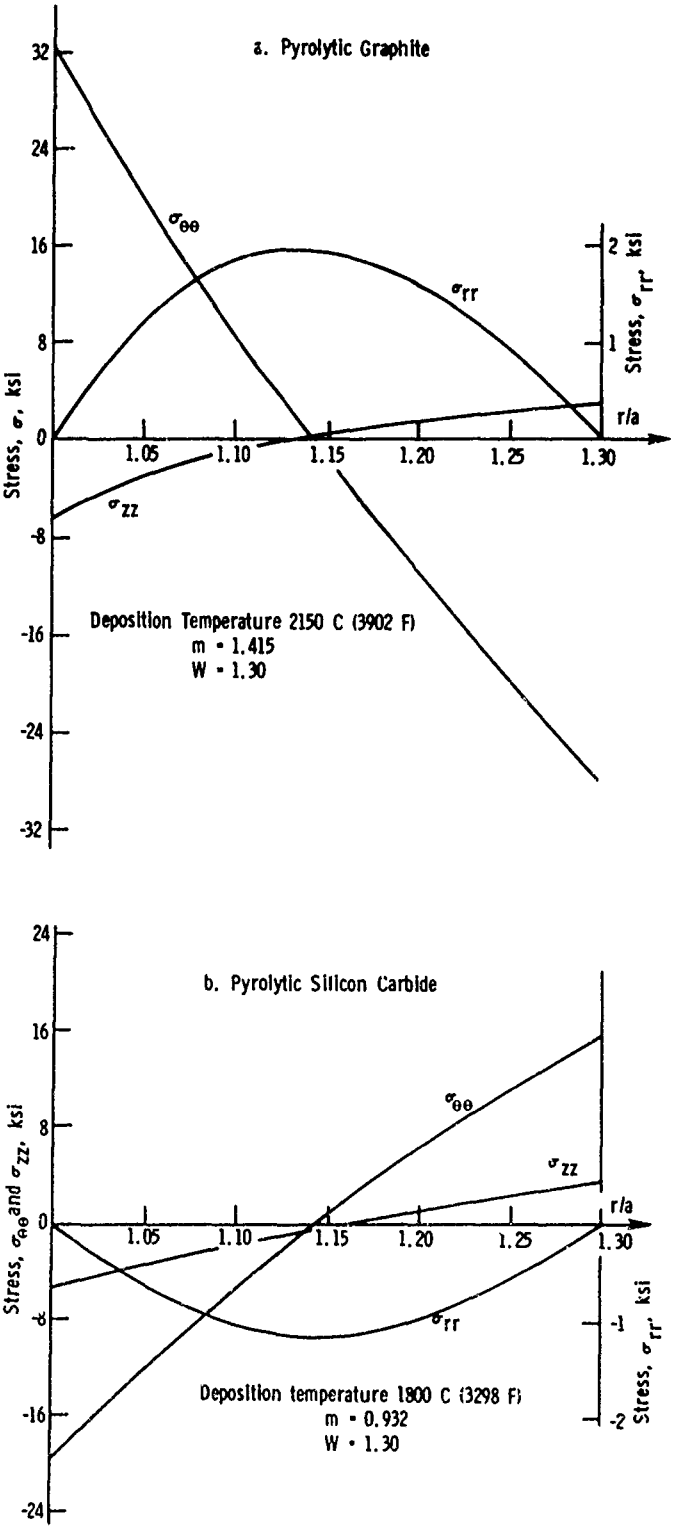

Figure 2. Residual stress distribution as a function of r/a for anisotropic thick hollow cylinders of (a) pyrolytic graphite and (b) pyrolytic silicon carbide.

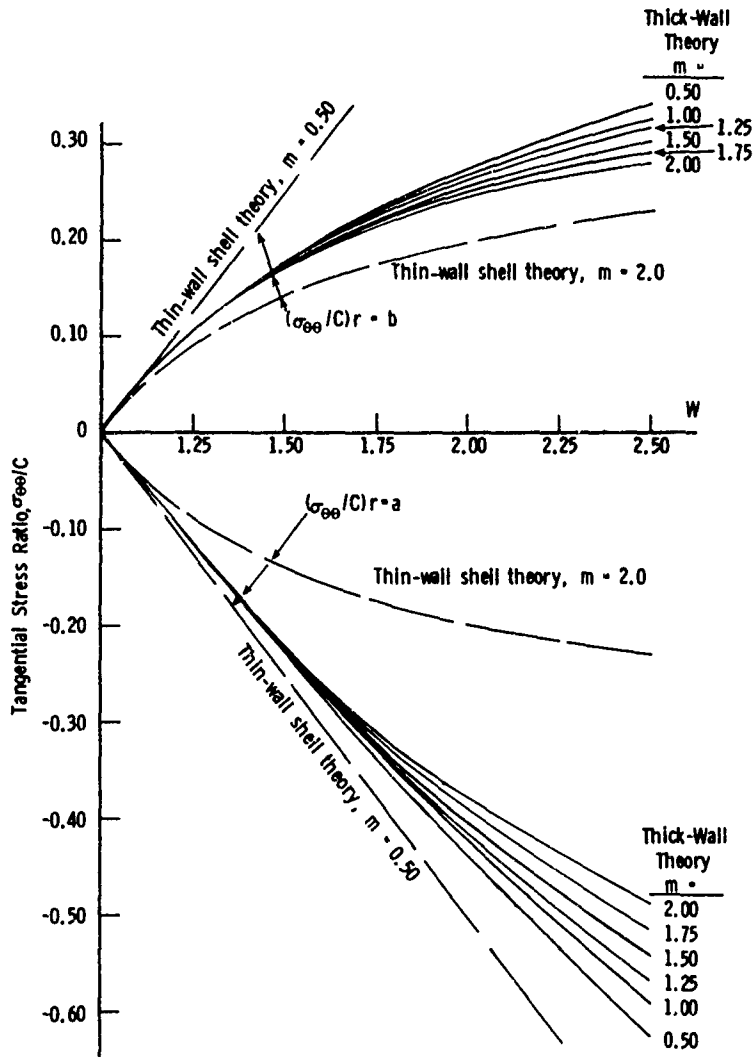

Figure 3. Tangential stress ratio at inner and outer radius as a function of the wall ratio W, and the anisotropy parameter m.

In Reference 14 the residual stresses in transversely anisotropic hexaferrite material during cooling were determined ignoring Poisson's ratios and axial deformation. This, of course, simplifies the analysis but dependent upon the material constants, the error could be extreme. For example, for the special case $\nu_{\theta\theta} = \nu_{\theta r} = 0$, $m = (E_{\theta\theta}/E_{rr})^{\frac{1}{2}}$, $C = (\beta_{rr}-\beta_{\theta\theta})E_{\theta\theta}$, and applying this approach, the stresses would differ from values calculated from more exact theory by -50% on a cylinder of pyrolytic graphite and -86% on one of pyrolytic silicon carbide.

Figure 4 presents the tangential and axial stresses at the inner and outer radii as well as the maximum radial stress as a function of the wall ratio for pyrolytic silicon carbide deposited at 1800 C (3272 F). The maximum radial

14. KOOLS, F. *Complications in Firing Oriented Hexaferrites Due to Anisotropic Effects Cracking of Radially Oriented Fringes During Firing.* Science of Ceramics, published by the Societe Francaise De Ceramique, v. 7, 1973, p. 27-45.

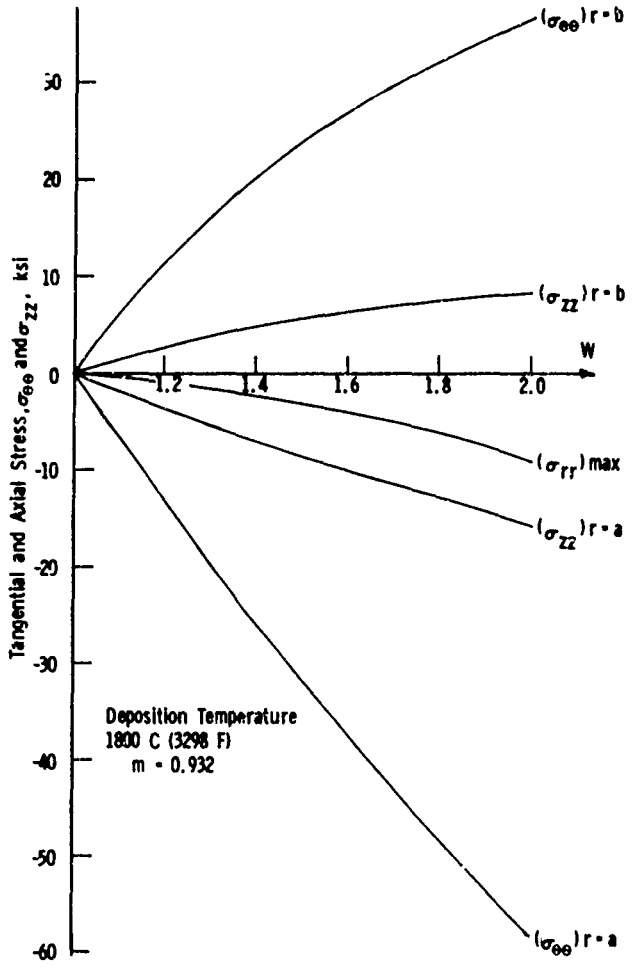

Figure 4. Residual tangential and axial stresses at the inner and outer radii and maximum radial stress for a thick hollow cylinder of pyrolytic silicon carbide as a function of the wall ratio W.

stress was determined by first obtaining the location of this stress from Equation 11 and using that value in Equation 2. The reader is cautioned that the stresses shown represent upper bounds in that it is assumed that the material is fully anisotropic. It appears from Figure 4 that the largest tensile stress will occur in the tangential direction at the outer radius of the cylinder. If the mechanism of differential-direction cooling due to anisotropy of CVD silicon carbide is the major cause of residual stress, then a longitudinal fracture will occur and originate at the outer radius. Thus, for a given material and deposition conditions there should result a critical wall ratio above which fracture will occur, see Reference 14.

In Section II the tangential and axial stress equations were simplified assuming the cylinder wall was thin, resulting in Equations 16 and 17. The stress

ratios $(\sigma_{\theta\theta}/C)_{r=a}$ and $(\sigma_{\theta\theta}/C)_{r=b}$ based on Equations 16 and 17 for m values of 0.50 and 2.00 are shown plotted as dashed lines in Figure 3 to facilitate comparison to the more exact theory given by the solid curves. It is readily seen that the differences between the more accurate thick-wall cylinder theory (solid curves) and the thin-wall cylinder theory (dashed lines) results can be quite extreme and depend upon the wall ratio W and the anisotropy parameter m.

IV. SUMMARY

1. The signs of the stresses are dependent upon the magnitudes of the directional contractions during cooling, β_{rr} and $\beta_{\theta\theta}$, and Poisson's ratios, $\nu_{\theta\theta}$ and $\nu_{\theta r}$.

2. Even if the contraction during cooling in the radial (β_{rr}) and tangential ($\beta_{\theta\theta}$) directions were equal, residual stresses would persist because of elastic anisotropy.

3. The absolute maximum stress which results from uniform cool-down is the tangential stress at the inner radius of the cylinder for all materials of transverse (orthotropic) anisotropy.

4. The maximum tensile stress for a fully anisotropic cylinder of pyrolytic silicon carbide material (α-SiC) occurs in the tangential direction at the outer radius. Fracture should originate at this location and extend in the longitudinal and radial directions. This mechanism should result in a critical wall ratio above which fracture will occur.

5. As the elastic anisotropic parameter m decreases the tangential stress increases when $W > 1.30$. If W is less than 1.30, m will have little effect on the magnitude of this stress.

6. If axial deformation and Poisson's ratios, $\nu_{\theta\theta}$ and $\nu_{\theta r}$, are ignored, errors in determining the residual stresses are dependent upon the properties of the material. The stresses would differ from those values calculated from more exact theory by approximately -50% for pyrolytic graphite and -86% for pyrolytic silicon carbide.

7. The differences between the thin-wall cylinder theory and the more accurate thick-wall cylinder theory results can be quite extreme and depend upon the wall ratio W and the anisotropic parameter m.

APPENDIX A. ANALYSIS

The geometry considered, as previously mentioned, is a long, thick hollow cylinder, as shown in Figure 1, with the three direction coordinates θ, r, and z. The hexagonal crystal structure is assumed to deposit at an elevated temperature in a preferred orientation in the radial direction such that there is isotropic symmetry about the Z-axis and anisotropy exists in the radial direction. It is also assumed that the elastic constants remain constant during deposition and subsequent cool-down is gradual such that the temperature throughout the cylinder is uniform. It is further assumed that there is no mechanical interaction between the substrate (mandrel) and deposit, i.e., no adhesion or no expansion coefficient mismatch. Also during deposition there is no temperature gradient occurring within the body (this problem can be solved separately).

According to Reference 15 the stress-strain relationships of such a body with cylindrical anisotropy is:

$$\left.\begin{aligned}
\varepsilon_{\theta\theta} &= (1/E_{\theta\theta})(\sigma_{\theta\theta}-\nu_{z\theta}\sigma_{zz})-(\nu_{r\theta}/E_{rr})\sigma_{rr} \\
\varepsilon_{rr} &= (1/E_{rr})\sigma_{rr}-(\nu_{\theta r}/E_{\theta\theta})\sigma_{\theta\theta}-(\nu_{zr}/E_{\theta\theta})\sigma_{zz} \\
\varepsilon_{zz} &= (1/E_{zz})\sigma_{zz}-(\nu_{\theta z}/E_{\theta\theta})\sigma_{\theta\theta}-(\nu_{rz}/E_{rr})\sigma_{rr}
\end{aligned}\right\} \qquad \text{(A-a)}$$

Notice, because of the conditions of symmetry, there are neither shear stresses nor shear strains. Also, since $E_{zz} = E_{\theta\theta}$, $\nu_{z\theta} = \nu_{\theta z} = \nu_{\theta\theta}$, $\nu_{r\theta} = \nu_{rz}$, $\nu_{zr} = \nu_{\theta r}$, and from the theorem of reciprocity we have $\nu_{r\theta}/E_{rr} = \nu_{\theta r}/E_{\theta\theta}$, thus:

$$\left.\begin{aligned}
\varepsilon_{\theta\theta} &= (1/E_{\theta\theta})(\sigma_{\theta\theta}-\nu_{\theta\theta}\sigma_{zz}-\nu_{\theta r}\sigma_{rr}) \\
\varepsilon_{rr} &= (1-E_{rr})[\sigma_{rr}-\nu_{r\theta}(\sigma_{\theta\theta}+\sigma_{zz})] \\
\varepsilon_{zz} &= (1-E_{\theta\theta})(\sigma_{zz}-\nu_{\theta\theta}\sigma_{\theta\theta}-\nu_{\theta r}\sigma_{rr})
\end{aligned}\right\} \qquad \text{(A-b)}$$

During uniform cool-down the contraction of the cylinder in the r direction is different than that either in the θ or z direction because of the differing thermal coefficients of expansion of the material. Thus, additional strain components must be added to Equation A-b as given in the following:

$$\left.\begin{aligned}
\varepsilon_{\theta\theta} &= (1/E_{\theta\theta})(\sigma_{\theta\theta}-\nu_{\theta\theta}\sigma_{zz}-\nu_{\theta r}\sigma_{rr})+\beta_{\theta\theta} \\
\varepsilon_{rr} &= (1/E_{rr})[\sigma_{rr}-\nu_{r\theta}(\sigma_{\theta\theta}+\sigma_{zz})]+\beta_{rr} \\
\varepsilon_{zz} &= (1/E_{\theta\theta})(\sigma_{zz}-\nu_{\theta\theta}\sigma_{\theta\theta}-\nu_{\theta r}\sigma_{rr})+\beta_{\theta\theta},
\end{aligned}\right\} \qquad \text{(A-c)}$$

where $\beta_{\theta\theta}$ and β_{rr} is the total contraction in the tangential and radial direction due to isothermal cool-down.

We shall first let $\varepsilon_{zz} = 0$ and later modify the solution to comply with an infinitely long cylinder with a stress-free end condition, thus Equation A-c becomes:

15. LEDHNITSKII, S. G. *Theory of Elasticity of an Anisotropic Elastic Body* in Holden-Day Series in Mathematical Physics. ed. by J. L. Brandstatter, 1963, p. 25.

$$\left.\begin{aligned}
&\sigma_{\theta\theta}-\nu_{\theta r}\sigma_{rr}-\nu_{\theta\theta}(\sigma_{zz})_{\varepsilon_{zz}=0} = \lambda_{\theta\theta}\\
&\nu_{r\theta}\sigma_{\theta\theta}-\sigma_{rr}+\nu_{r\theta}(\sigma_{zz})_{\varepsilon_{zz}=0} = \lambda_{rr}\\
&\nu_{\theta\theta}\sigma_{\theta\theta}+\nu_{\theta r}\sigma_{r}-(\sigma_{zz})_{\varepsilon_{zz}=0} = \lambda
\end{aligned}\right\} \qquad \text{(A-d)}$$

where

$$\lambda_{\theta\theta} = (\varepsilon_{\theta\theta}-\beta_{\theta\theta})E_{\theta\theta}$$

$$\lambda_{rr} = -(\varepsilon_{rr}-\beta_{rr})E_{rr}, \text{ and}$$

$$\lambda = \beta_{\theta\theta}E_{\theta\theta}$$

Equation A-d can be solved such that the normal stresses $\sigma_{\theta\theta}$, σ_{rr}, and σ_{zz} can be expressed in explicit form; when this is accomplished we have:

$$\left.\begin{aligned}
\sigma_{\theta\theta} &= (1/D)[(1-\nu_{\theta r}\nu_{r\theta})\lambda_{\theta\theta}-\nu_{\theta r}(1+\nu_{\theta\theta})\lambda_{rr}-(\nu_{\theta\theta}+\nu_{\theta r}\nu_{r\theta})\lambda]\\
\sigma_{rr} &= (1+\nu_{\theta\theta})/D[\nu_{r\theta}\lambda_{\theta\theta}-(1-\nu_{\theta\theta})\lambda_{rr}-\nu_{r\theta}\lambda]\\
(\sigma_{zz})_{\varepsilon_{zz}=0} &= (1/D)[(\nu_{\theta\theta}+\nu_{r\theta}\nu_{\theta r})\lambda_{\theta\theta}-(1+\nu_{\theta\theta})\nu_{\theta r}\lambda_{rr}-(1-\nu_{r\theta}\nu_{\theta r})\lambda]
\end{aligned}\right\} \qquad \text{(A-e)}$$

where

$$D = (1+\nu_{\theta\theta})(1-\nu_{\theta\theta}-2\nu_{\theta r}\nu_{r\theta})$$

The equilibrium equation for deformation symmetrical about the axis of a thick-walled cylinder[16] is:

$$d\sigma_{rr}/dr+(\sigma_{rr}-\sigma_{\theta\theta})/r = 0 \qquad \text{(A-f)}$$

and also by definition:

$$\varepsilon_{\theta\theta} = u/r, \text{ and}$$

$$\varepsilon_{rr} = du/dr$$

It is assumed that the constants $\beta_{\theta\theta}$, β_{rr}, $E_{\theta\theta}$, and E_{rr} are not functions of the radius. Therefore, by differentiating σ_{rr} with respect to r from the second of Equations A-e and substituting that result as well as the relationships for $\sigma_{\theta\theta}$ and σ_{rr} from Equation A-d into Equation A-f gives:

$$r^2d^2u/dr^2+rdu/dr-m^2u = a_1r \qquad \text{(A-1)}$$

where

$$m^2 = (E_{\theta\theta}/E_{rr})(1-\nu_{\theta r}\nu_{r\theta})/(1-\nu_{\theta\theta}^2), \text{ and}$$

$$a_1 = (1/1-\nu_{\theta\theta})[(1-\nu_{\theta\theta}-\nu_{\theta r})\beta_{rr}-(1-2\nu_{r\theta})(E_{\theta\theta}/E_{rr})\beta_{\theta\theta}]$$

Equation A-1 is an equidimensional linear differential equation, which is variously called Euler's equation or Cauchy's equation,[7] whose homogeneous solution is:

16. TIMOSHENO, S., and GOODIER, J. N. *Theory of Elasticity*, 2nd ed. McGraw-Hill Book Co., Inc., 1951, p. 236.

$$u_h = C_1 r^m + C_2/r^m,$$

and the particular solution is

$$u_p = a_1 r/(1-m^2),\ m \neq 1.0.$$

Also note that in the above solution it is assumed that $\nu_{\theta r}\nu_{r\theta} < 1.0$. The complete solution is:

$$u = C_1 r^m + C_2/r^m + a_1 r/(1-m^2),\ m \neq 1.0. \tag{A-2}$$

C_1 and C_2 are obtained from the boundary conditions, i.e., $\sigma_{rr} = 0$ when $r = a$ and b. The constants C_1 and C_2 are determined through the use of the middle equation σ_{rr} of Equation A-e, Equation A-2, the appropriate strain definitions, and the boundary conditions. When this is accomplished one determines the following equations for C_1 and C_2:

$$C_1 = \frac{C[(1-\nu_{\theta\theta})E_{\theta\theta}/E_{rr}-2\nu_{\theta r}^2](W^{m+1}-1)a^{1-m}}{E_{\theta\theta}(1-m^2)[\nu_{\theta r}+(1-\nu_{\theta\theta})m](1-W^{2m})}$$

and

$$C_2 = \frac{C[(1-\nu_{\theta\theta})E_{\theta\theta}/E_{rr}-2\nu_{\theta r}^2](W^{m-1}-1)b^{m+1}}{E_{\theta\theta}(1-m^2)[\nu_{\theta r}+(1-\nu_{\theta\theta})m](1-W^{2m})}$$

where

$$C = [\beta_{rr}-(1+\nu_{\theta\theta}-\nu_{\theta r})\beta_{\theta\theta}]E_{\theta\theta}/(1-\nu_{\theta\theta}^2)$$

Substitution of C_1 and C_2 into Equation A-2 and dividing by the variable r, gives

$$\varepsilon_{\theta\theta} = u/r = \frac{C[(1-\nu_{\theta\theta})E_{\theta\theta}/E_{rr}-2\nu_{\theta r}^2]}{E_{\theta\theta}(1-m^2)(1-W^{2m})}\left\{\frac{(W^{m+1}-1)}{\nu_{\theta r}+(1-\nu_{\theta\theta})m}(r/a)^{m-1}\right. \tag{A-3}$$

$$\left. + \frac{(W^{m-1}-1)}{[\nu_{\theta r}-(1-\nu_{\theta\theta})m]}\frac{W^{m+1}}{(r/a)^{m+1}}\right\} + a_1/(1-m^2)$$

and by differentiating Equation A-2 with respect to r, and substituting for C_1 and C_2 from the above, the radial strain ε_{rr} can be obtained, which is:

$$\varepsilon_{rr} = du/dr = \frac{mC[(1-\nu_{\theta\theta})E_{\theta\theta}/E_{rr}-2\nu_{\theta r}^2]}{E_{\theta\theta}(1-m^2)(1-W^{2m})}\left\{\frac{(W^{m+1}-1)}{[\nu_{\theta r}+(1-\nu_{\theta\theta})m]}(r/a)^{m-1}\right. \tag{A-4}$$

$$\left. - \frac{(W^{m-1}-1)}{[\nu_{\theta r}-(1-\nu_{\theta\theta})m]}\frac{W^{m+1}}{(r/a)^{m+1}}\right\} + a_1/(1-m^2)$$

Through the use of Equation A-e and the definitions of strains, the tangential, radial, and axial stresses (with $\varepsilon_{zz} = 0$) can be obtained and are:

$$\sigma_{\theta\theta} = C/(1-m^2)\left\{1+m/(1-W^{2m})\left[(W^{m+1}-1)(r/a)^{m-1}-(W^{m-1}-1)W^{m+1}/(r/a)^{m+1}\right]\right\} \quad \text{(A-5)}$$

$$\sigma_{rr} = C/(1-m^2)\left\{1+1/(1-W^{2m})\left[(W^{m+1}-1)(r/a)^{m-1}+(W^{m-1}-1)W^{m+1}/(r/a)^{m+1}\right]\right\} \quad \text{(A-6)}$$

$$(\sigma_{zz})_{\varepsilon_{zz}=0} = (1+\nu_{\theta\theta})/D\left\{(\nu_{\theta\theta}M_{\theta\theta}+\nu_{r\theta}M_{rr})C_1 r^{m-1}/(1-m^2)+\right.$$
$$\left.[(\nu_{\theta\theta}N_{\theta\theta}+\nu_{r\theta}N_{rr})/(1-m^2)]C_2/r^{m+1}+(\nu_{\theta\theta}P_{\theta\theta}+\nu_{r\theta}P_{rr})E_{\theta\theta}\right\}-\nu_{\theta\theta}E_{\theta\theta} \quad \text{(A-7a)}$$

where

$$M_{\theta\theta} = (1-\nu_{\theta r}\nu_{r\theta})/(1+\nu_{\theta\theta})+m\nu_{r\theta}, \quad N_{\theta\theta} = (1-\nu_{\theta r}\nu_{r\theta})/(1+\nu_{\theta\theta})-m\nu_{r\theta}$$

$$M_{rr} = \nu_{\theta r}+(1-\nu_{\theta\theta})m, \qquad N_{rr} = \nu_{\theta r}-(1-\nu_{\theta\theta})m$$

$$P_{\theta\theta} = [(1-\nu_{\theta r}\nu_{r\theta})/(1+\nu_{\theta\theta})+\nu_{r\theta}]a_1/(1-m^2)-(\beta_{\theta\theta}+\nu_{r\theta}\beta_{rr}), \text{ and}$$

$$P_{rr} = [C/E_{\theta\theta}(1-m^2)][(1-\nu_{\theta\theta})E_{\theta\theta}/E_{rr}-2\nu_{\theta r}^2].$$

The axial stress σ_{zz} can now be determined such that the stress at the ends of the cylinder vanish. This is accomplished by obtaining a resulting force C_3 in the following manner:

$$C_3\pi(b^2-a^2) = -\int_a^b 2(\sigma_{zz})_{\varepsilon_{zz}=0}\pi r dr$$

Substitution of $(\sigma_{zz})_{\varepsilon_{zz}=0}$ from Equation A-7a into the above, integrating and solving for C_3 results in:

$$C_3 = \left[\frac{-2(1+\nu_{\theta\theta})}{D}\right]\left\{\left[\frac{\nu_{\theta\theta}M_{\theta\theta}+\nu_{r\theta}M_{rr}}{(1-m^2)(1+m)}\right]\frac{(W^{m+1}-1)}{(W^2-1)}\frac{C_1}{a^{1-m}}\right. \quad \text{(A-7b)}$$

$$+\left[\frac{\nu_{\theta\theta}N_{\theta\theta}+\nu_{r\theta}N_{rr}}{(1-m^2)(1-m)}\right]\frac{(W^{1-m}-1)}{(W^2-1)}(W)^{m+1}\frac{C_2}{b^{1+m}}$$

$$\left.+\frac{E_{\theta\theta}}{2}\left(\nu_{\theta\theta}P_{\theta\theta}+\nu_{r\theta}P_{rr}-\frac{\beta_{\theta\theta}D}{1+\nu_{\theta\theta}}\right)\right\}$$

Now by adding C_3, given by Equation A-7b, to $(\sigma_{zz})_{\varepsilon_{zz}=0}$, given by Equation A-7a and noting that $M_{\theta\theta}/M_{rr} = mE_{rr}/E_{\theta\theta}$, and $N_{\theta\theta}/N_{rr} = -mE_{rr}/E_{\theta\theta}$,

we obtain σ_{zz}, which is:

$$\sigma_{zz} = \frac{C}{(1-m^2)(1-W^{2m})}\left\{(\nu_{\theta r}+m\nu_{\theta\theta})(W^{m+1}-1)\left[(r/a)^{m-1} - \frac{2}{(1+m)}\frac{(W^{1-m}-1)}{(W^2-1)}\right]\right. \tag{A-7}$$

$$\left. +(\nu_{\theta r}-m\nu_{\theta\theta})(W^{m-1}-1)W^{m+1}\left[\frac{1}{(r/a)^{m+1}} - \frac{2}{(1-m)}\frac{(W^{1-m}-1)}{(W^2-1)}\right]\right\}$$

Now the axial strain ε_{zz} can be obtained by substitution of Equations A-5, A-6, and A-7 into the last of Equation A-c. This results in:

$$\varepsilon_{zz} = \beta_{\theta\theta} - C\frac{(\nu_{\theta\theta}+\nu_{\theta r})}{E_{\theta\theta}(1-m^2)} - \frac{2C}{E_{\theta\theta}(1-m^2)(1-W^{2m})(W^2-1)}\left[\left(\frac{\nu_{\theta r}+m\nu_{\theta\theta}}{1+m}\right)\left(W^{1+m}-1\right)^2\right. \tag{A-8}$$

$$\left. +\left(\frac{\nu_{\theta r}-m\nu_{\theta\theta}}{1-m}\right)\left(W^{m-1}-1\right)\left(W^{1-m}-1\right)W^{m+1}\right]$$

Equations A-3 and A-4 give the tangential and radial strains as a function of the radius ratio parameter r/a, the wall ratio, and the various elastic and physical constants. The axial strain given by Equation A-8 is constant and dependent only upon the wall ratio and the elastic and physical parameters.

Equations A-5, A-6, and A-7 gives the tangential, radial, and axial stress $\sigma_{\theta\theta}$, σ_{rr}, and σ_{zz} as a function of the radius ratio parameter r/a, the wall ratio W, and the various elastic and physical constants.

The stresses and strains at the inner and outer radii can readily be obtained by allowing r = a and r = b in the appropriate equations. The tangential and axial stresses at the inner and outer radii are obtained from Equations A-5 and A-7 and are:

$$(\sigma_{\theta\theta})_{r=a} = \left(\frac{C}{1-m^2}\right)\left[1+\left(\frac{m}{1-W^{2m}}\right)\left(2W^{m+1}-1-W^{2m}\right)\right], \tag{A-9}$$

$$(\sigma_{\theta\theta})_{r=b} = \left(\frac{C}{1-m^2}\right)\left[1-\left(\frac{m}{1-W^{2m}}\right)\left(2W^{m-1}-1-W^{2m}\right)\right], \tag{A-10}$$

$$(\sigma_{zz})_{r=a} = \frac{C}{(1-m^2)(1-W^{2m})}\left\{(\nu_{\theta r}+m\nu_{\theta\theta})(W^{m+1}-1)\left[1-\left(\frac{2}{1+m}\right)\frac{(W^{m+1}-1)}{(W^2-1)}\right]\right. \tag{A-11}$$

$$\left. +(\nu_{\theta r}-m\nu_{\theta\theta})(W^{m-1}-1)W^{m-1}\left[1-\left(\frac{2}{1-m}\right)\frac{(W^{1-m}-1)}{(W^2-1)}\right]\right\},$$

and

$$(\sigma_{zz})_{r=b} = \frac{C}{(1-m^2)(1-W^{2m})}\left\{(\nu_{\theta r}+m\nu_{\theta\theta})(W^{m+1}-1)\left[W^{m-1}-\left(\frac{2}{1+m}\right)\frac{(W^{m+1}-1)}{(W^2-1)}\right]\right.$$
$$\left.+(\nu_{\theta r}-m\nu_{\theta\theta})(W^{m-1}-1)\left[1-\left(\frac{2}{1-m}\right)\frac{(W^{1-m}-1)}{(W^2-1)}\,W^{m+1}\right]\right\} \qquad \text{(A-12)}$$

The tangential and radial strains at the inner and outer radii obtained from Equations A-3 and A-4 are:

$$(\varepsilon_{\theta\theta})_{r=a} = \frac{C[(1-\nu_{\theta\theta})E_{\theta\theta}/E_{rr}-2\nu_{\theta r}^2]}{E_{\theta\theta}(1-W^{2m})(1-m^2)}\left\{\frac{(W^{m+1}-1)}{\nu_{\theta r}+(1-\nu_{\theta\theta})m}+\frac{(W^{m-1}-1)W^{m+1}}{\nu_{\theta r}-(1-\nu_{\theta\theta})m}\right\}+\frac{a_1}{1-m^2}, \qquad \text{(A-13)}$$

$$(\varepsilon_{\theta\theta})_{r=b} = \frac{C[(1-\nu_{\theta\theta})E_{\theta\theta}/E_{rr}-2\nu_{\theta r}^2]}{E_{\theta\theta}(1-W^{2m})(1-m^2)}\left\{\frac{(W^{m+1}-1)W^{m-1}}{\nu_{\theta r}+(1-\nu_{\theta\theta})m}+\frac{(W^{m-1}-1)}{\nu_{\theta\theta}-(1-\nu_{\theta\theta})m}\right\}+\frac{a_1}{1-m^2}, \qquad \text{(A-14)}$$

$$(\varepsilon_{rr})_{r=a} = \frac{mC[(1-\nu_{\theta\theta})E_{\theta\theta}/E_{rr}-2\nu_{\theta r}^2]}{E_{\theta\theta}(1-W^{2m})(1-m^2)}\left\{\frac{(W^{m+1}-1)}{\nu_{\theta r}+(1-\nu_{\theta\theta})m}-\frac{(W^{m-1}-1)W^{m+1}}{\nu_{\theta r}-(1-\nu_{\theta\theta})m}\right\}+\frac{a_1}{1-m^2}, \qquad \text{(A-15)}$$

and

$$(\varepsilon_{rr})_{r=b} = \frac{mC[(1-\nu_{\theta\theta})E_{\theta\theta}/E_{rr}-2\nu_{\theta r}^2]}{E_{\theta\theta}(1-W^{2m})(1-m^2)}\left\{\frac{(W^{m+1}-1)W^{m-1}}{\nu_{\theta r}+(1-\nu_{\theta\theta})m}-\frac{(W^{m-1}-1)}{\nu_{\theta r}-(1-\nu_{\theta\theta})m}\right\}+\frac{a_1}{1-m^2} \qquad \text{(A-16)}$$

Since ε_{zz} as given by Equation A-7 is constant, there is no difference in axial strain at the inner and outer radii.

Examination of the stress equations for $\sigma_{\theta\theta}$ and σ_{zz} reveals that the absolute maximum stress occurs at the inner radius, i.e., when $r = a$.

The location at which the radial stress is a maximum can be found by maximizing Equation A-6. If this is accomplished we obtain:

$$r/a = \left[\left(\frac{m+1}{m-1}\right)\frac{(W^{m-1}-1)}{(W^{m+1}-1)}\,W^{m+1}\right]^{\frac{1}{2m}} \qquad \text{(A-17)}$$

APPENDIX B. THIN WALL STRESSES

The residual stresses $\sigma_{\theta\theta}$ and σ_{zz} at the inner and outer radii of a thin-walled cylinder can be obtained from Equations A-9 and A-10, and A-11 and A-12. This is accomplished by letting $W = 1+t/a$ where t is the cylinder wall thickness and using series expansions for each of the terms that appear in Equations A-9 to A-12. For example, the reduction of Equation A-9 to thin-wall cylinder theory is accomplished in the following manner:

Note:

$$(\sigma_{\theta\theta})_{r=a} = (C/1-m^2)[1+(m/1-W^{2m})(2W^{m+1}-1-W^{2m})], \text{ and}$$

by using a series expansion for W^{2m} and W^{m+1}, i.e.:

$$W^{2m} = (1+t/a)^{2m} = 1+2mt/a+m(2m-1)(t/a)^2+\ldots\ldots, \quad (t/a)^2 < 1, \text{ and}$$

$$W^{m+1} = (1+t/a)^{m+1} = 1+(m+1)t/a+m(m+1)(t/a)^2/2+\ldots\ldots, \quad (t/a)^2 < 1,$$

and substituting the appropriate series expansion (only up to the second-order terms) into the above equation as shown below gives:

$$(\sigma_{\theta\theta})_{r=a} = \left(\frac{C}{1-m^2}\right)\left\{1-\frac{m[2(1+(m+1)t/a+m(m+1)/2(t/a)^2)-1-(1+2mt/a+m(2m-1))(t/a)]}{2m(t/a)+m(2m-1)(t/a)^2}\right\}$$

The above reduces to:

$$(\sigma_{\theta\theta})_{r=a} = -C(t/a)/[2+(2m-1)t/a], \tag{B-1}$$

Utilizing the same approach the remaining desired equations are:

$$(\sigma_{\theta\theta})_{r=b} = C(t/a)/[2+(2m-1)t/a], \tag{B-2}$$

$$(\sigma_{zz})_{r=a} = -\nu_{\theta\theta}C(t/a)/2(1+mt/a), \tag{B-3}$$

and finally:

$$(\sigma_{zz})_{r=b} = \nu_{\theta\theta}C(t/a)/2(1+mt/a) \tag{B-4}$$

APPENDIX C. ELASTIC AND PHYSICAL CONSTANTS

The elastic constants for two transversely anisotropic materials, pyrolytic graphite and pyrolytic silicon carbide, were used in the body of the report to obtain numerical results. Pyrolytic graphite was chosen because its property data are well documented, see, for example, References 5, 8, and 9. Pyrolytic silicon carbide was also considered because it is a material of potential promise. Unfortunately, a search of the literature revealed that there were no anisotropic property data available for the other material of interest, pyrolytic silicon nitride. Even though the pyrolytic silicon carbide data from the literature were incomplete the anisotropic elastic constants were estimated indirectly from Reference 10.

The data for pyrolytic graphite data are first presented and then that data for pyrolytic silicon carbide follow.

The anisotropic elastic constants utilized for calculations were those obtained from Reference 8 as:

$E_{\theta\theta} = 4.29 \times 10^6$ psi (29.58×10^3 MN/m^2), $\nu_{\theta\theta} = -0.15$

$E_{rr} = 1.55 \times 10^6$ psi (10.69×10^3 MN/m^2), $\nu_{\theta r} = +0.90$

Although the published value for $\nu_{r\theta}$ is 0.35, for consistency the reciprocating relationship was used, resulting in $\nu_{r\theta} = 0.325$. This value was used throughout the calculations. Recalling that:

$$m = [(E_{\theta\theta}/E_{rr})(1-\nu_{\theta r}\nu_{r\theta})/(1-\nu_{\theta\theta}^2)]^{1/2}$$

and substituting the above constants into this relationship gives:

$$m = 1.415$$

The total contraction during cooling in the tangential and radial directions was determined from Reference 9 as

$$\beta_{\theta\theta} = \alpha_1 + \alpha_2(T_a - T_d)$$

where

$$\alpha_1 = -270 \times 10^{-6} \text{ in./in.}$$

and

$$\alpha_2 = 1.13 \times 10^{-6} \text{ in./(in.-°F)},$$

thus

$$\beta_{\theta\theta} = -270 \times 10^{-6} \text{ in./in.} + [1.13 \times 10^{-6} \text{ in./(in.-°F)}](70 - 3902 \text{ F}), \text{ or}$$

$$\beta_{\theta\theta} = -4600 \times 10^{-6} \text{ in./in.}$$

also

$$\beta_{rr} = \alpha_3(T_a - T_d),$$

where

$$\alpha_3 = 13.50 \times 10^{-6} \text{ in./(in.-°F)},$$

and

$$\beta_{rr} = [13.50 \times 10^{-6} \text{ in./(in.-°F)}](70 \text{ F-3902 F}), \text{ or}$$

$$\beta_{rr} = -51{,}700 \times 10^{-6} \text{ in./in.}$$

The manner by which the elastic and physical constants for silicon carbide (CVD) were calculated are now presented in the following.

The authors of Reference 10 determined by resonance and the double-pulse echo method for the hexagonal crystal structure (α-SiC 6H (33)) the magnitude of the stiffnesses c_{11}, c_{12}, c_{44}, c_{33}, and c_{66} and the compliances s_{11}, s_{12}, s_{44} and s_{66}. Unfortunately, no values were reported for c_{13}, s_{13}, and s_{33}. However, according to Reference 11 there is an interconversion between the stiffnesses and the compliances of a hexagonal system. Through the use of three simultaneous equations, the three unknowns c_{13}, s_{13}, and s_{33} were calculated. Using nominal experimental values of the known parameters, s_{13} was found to be an imaginary number, which can not physically occur. Closer examination of the errors associated with the experimentally determined constants published in Reference 10 revealed that extremely large errors would result in the calculation of c_{13}, s_{13}, and s_{33} when using the interconversion equations. However, the elastic constants of other polytypes of SiC are not likely to be very different and have included calculated values of the transformed elastic constants of a cubic polytype β-SiC.[10] Although this system is trigonal rather than hexagonal, mean values of the transformed stiffnesses compare quite well to those experimentally determined stiffnesses for the hexagonal structure. These transformed values of the stiffnesses for the trigonal system were used here in conjunction with the interconversion equations for a trigonal system[11] to determine the compliances. These calculations and the results are summarized below.

The interconversion equations are:

(a) $c_{11}+c_{12} = s_{33}/X_1$

(b) $c_{13} = -s_{13}/X_1$

(c) $c_{33} = (s_{11}+s_{12})/X_1$

(d) $X_1 = s_{33}(s_{11}+s_{12})-2s_{13}^2$

(e) $c_{11}-c_{12} = s_{44}/X_2$

(f) $c_{14} = -s_{14}/X_2$

(g) $c_{44} = (s_{11}-s_{12})/X_2$

(h) $X_2 = s_{44}(s_{11}-s_{12})-2s_{14}^2$

Reworking these equations so that they are amenable for use, we obtain:

$$s_{13} = -[c_{13}/(c_{11}+c_{12})]s_{33} \qquad s_{12} = -s_{11}-2s_{13}^2/(1/c_{33}-s_{33})$$

$$s_{33} = 1/[c_{33}-2c_{13}^2/(c_{11}+c_{12})] \qquad s_{11} = -s_{13}^2/(1/c_{33}-s_{33})-s_{14}^2/(1/c_{44}-s_{44})$$

$$s_{44} = 1/[c_{44}-2c_{14}^2/(c_{11}-c_{12})] \qquad s_{14} = -[c_{14}/(c_{11}-c_{12})]s_{44}$$

The transformed stiffnesses,[10] given in 10^{12}dyn/cm^2, are:

$c_{11} = 4.793$ $\quad$ $c_{14} = 0.598$

$c_{12} = 0.981$ $\quad$ $c_{33} = 5.214$

$c_{13} = 0.558$ $\quad$ $c_{44} = 1.483$

By utilizing the above equations the corresponding compliances given in units of 10^{-13}cm^2/dynes, are:

$s_{11} = 2.392$ $\quad$ $s_{14} = 1.211$

$s_{12} = -0.610$ $\quad$ $s_{33} = 1.958$

$s_{13} = -0.189$ $\quad$ $s_{44} = 7.72$

The remaining elastic constants were determined from the above and are given below:

$E_{\theta\theta} = 1/s_{11} = 60.6 \times 10^6$ psi $(417.82 \times 10^3$ MN/m$^2)$

$E_{rr} = 1/s_{33} = 74.1 \times 10^6$ psi $(510.90 \times 10^3$ MN/m$^2)$

$\nu_{\theta\theta} = \nu_{12} = -s_{12}/s_{11} = +0.255$

$\nu_{\theta r} = \nu_{13} = -s_{13}/s_{11} = +0.079$

and

$\nu_{r\theta} = \nu_{\theta r} = E_{rr}/E_{\theta\theta} = 0.097$

Finally, m was determined from the above values to be 0.932.

Reference 12 gives the thermal expansion curves in the basal direction "a" and in the "c" direction as a function of temperature for the hexagonal silicon carbide system (mod II). These curves were used to determine the total shrinkage in the θ and r directions of SiC from 1800 C to room temperature and were found to be

$\beta_{\theta\theta} = -9624 \times 10^{-6}$ in./in.,

and

$\beta_{rr} = -9204 \times 10^{-6} \times 10^{-6}$ in./in.

DISTRIBUTION LIST

No. of Copies	To
	Office of the Director, Defense Research and Engineering, The Pentagon, Washington, D. C. 20301
1	ATTN: Mr. R. M. Standahar
12	Commander, Defense Documentation Center, Cameron Station, Building 5, 5010 Duke Street, Alexandria, Virginia 22314
	Advanced Research Projects Agency, 1400 Wilson Blvd., Arlington, Virginia 22209
1	ATTN: Director
1	Dr. Stickley, Director of Materials Sciences
	Metals and Ceramics Information Center, Battelle Columbus Laboratories, 505 King Avenue, Columbus, Ohio 43201
2	ATTN: Mr. Daniel Maykuth
	Deputy Chief of Staff, Research, Development, and Acquisition Headquarters, Department of the Army, Washington, D. C. 20310
1	ATTN: DAMA-ARZ
1	Dr. Bernard R. Stein
1	Dr. James I. Bryant, DARD-ARS-PM
	Commander, Army Research Office, P.O. Box 1211, Research Triangle Park, North Carolina 27709
1	ATTN: Information Processing Office
	Commander, U. S. Army Materiel Development and Readiness Command, 5001 Eisenhower Avenue, Alexandria, Virginia 22333
1	ATTN: DRCLDC, Mr. R. Zentner
1	DRCRD-DE, Development Division
1	DRCRD-RS, Research Division
1	DRCRD-RS, Scientific Deputy
	Commander, U. S. Army Communications Research and Development Command, Fort Monmouth, New Jersey 07703
1	ATTN: DRDCO-GG-TD
1	DRDCO-GG-DM
	Commander, U. S. Army Aviation Systems Command, P. O. Box 209, Main Office, St. Louis, Missouri 63166
1	ATTN: DRSAV-LEP, Mr. J. M. Thorp
1	DRSAV-ER, Dr. I. Peterson
1	R. Long, Deputy Director, RD&E
	Commander, U. S. Army Missile Research and Development Command, Redstone Arsenal, Alabama 35809
1	ATTN: Technical Library
1	DRSMI-RKK, Mr. C. Martens, Bldg. 7120
1	DRSMI-RSM, Mr. E. J. Wheelahan
1	DRSMI-IE, Mr. J. E. Kirshtein
1	DRSMI-R, Mr. John L. McDaniel
1	DRSMI-RBLD, Redstone Scientific Information Center
1	Chief Scientist, Dr. W. W. Carter
1	Directorate of R&D
1	Dr. B. Steverding
	Commander, U. S. Army Natick Research and Development Command, Natick, Massachusetts 01760
1	ATTN: Technical Library
1	Dr. E. W. Ross
1	DRXNA-UE, Dr. L. A. McClaine
	Commander, U. S. Army Satellite Communications Agency, Fort Monmouth, New Jersey 07703
1	ATTN Technical Document Center
	Commander, U. S. Army Mobility Equipment Command, 4300 Goodfellow Boulevard, St. Louis, Missouri 63120
1	ATTN: DRSME-PLC, Mr. J. Murphy
	Commander, U. S. Army Tank-Automotive Research and Development Command, Warren, Michigan 48090
1	ATTN: DRDTA-RKA
2	DRDTA-UL, Technical Library
1	DRDTA-PPS, Mr. David Siegel
1	Mr. J. P. Jones
1	DRDTA-BSL
	Commander, U. S. Army Armament Research and Development Command, Dover, New Jersey 07801
2	ATTN: Technical Library
1	DRDAR-SC, Dr. C. M. Hudson
1	DRDAR-PPW-P8, Mr. Francis X. Walter
	Commander, White Sands Missile Range, New Mexico 88002
1	ATTN: SLEWS-WS-VT
	Commander, Aberdeen Proving Ground, Maryland 21005
1	ATTN STEAP-TL, Bldg. 305
	Commander, Frankford Arsenal, Philadelphia, Pennsylvania 19137
1	ATTN Library, M1300, Bl. 51-2
1	Dr. C. M. Carman
1	Mr. J Kymer
1	Mr. M Schwartz
1	Pitman-Dunn Institute of Research

No. of Copies	To
	Commander, U. S. Army Ballistic Research Laboratory, Aberdeen Proving Ground, Maryland 21005
1	ATTN: Dr. J. Frasier
1	Dr. R. Vitali
1	Dr. G. L. Filbey
1	Dr. R. Karpp
1	Dr. W. Gillich
1	Dr. D. Eichelberger
	Commander, Harry Diamond Laboratories, 2800 Powder Mill Road, Adelphi, Maryland 20783
1	ATTN: Technical Information Office
	Commander, Picatinny Arsenal, Dover, New Jersey 07801
1	ATTN: SARPA-RT-S
1	Mr. J. Pearson
1	Dr. E. N. Clark
1	Mr. A. Garcia
1	Feltman Research Laboratories
	Commander, Rock Island Arsenal, Rock Island, Illinois 61201
1	ATTN: SARRI-RDL
	Commander, Redstone Scientific Information Center, U. S. Army Missile Command, Redstone Arsenal, Alabama 35809
4	ATTN: DRSMI-RBLD, Document Section
	Commander, Watervliet Arsenal, Watervliet, New York 12189
1	ATTN: Dr. T. Davidson
1	Mr. D. P. Kendall
1	Mr. J. F. Throop
1	SARWV-RDR, Dr. F. W. Schmiedeshoff
1	SARWV-R
1	Dr. Robert Weigle
	Commander, U. S. Army Foreign Science and Technology Center, 220 7th Street, N. E., Charlottesville, Virginia 22901
1	ATTN: Military Tech, Mr. Marley
	Director, Eustis Directorate, U. S. Army Air Mobility Research and Development Laboratory, Fort Eustis, Virginia 23604
1	ATTN: Mr. J. Robinson, SAVDL-E-MOS (AVRADCOM)
1	J. White, Assistant Technical Director
	Director, U. S. Army Materiel Systems Analysis Activities Aberdeen Proving Ground, Maryland 21005
1	ATTN: DRXSY-D
	Commander, U. S. Army Armament Research and Development Command, Dover, New Jersey 07801
1	ATTN: DRDAR-SCM, J. D. Corrie
	Commander, U. S. Army Armament Research and Development Command, Aberdeen Proving Ground, Maryland 21010
1	ATTN: DRDAR-QAC-E
	U S. Army Aviation Training Library, Fort Rucker, Alabama 36362
1	ATTN: Building 5906-5907
	Commander, U. S. Army Agency for Aviation Safety, Fort Rucker, Alabama 36362
1	ATTN: Librarian, Bldg. 4905
	Commander, USACDC Air Defense Agency, Fort Bliss, Texas 79916
1	ATTN: Technical Library
	Commander, U. S. Army Engineer School, Fort Belvoir, Virginia 22060
1	ATTN: Library
	Commander, U. S. Army Engineer Waterways Experiment Station, Vicksburg, Mississippi 39180
1	ATTN: Research Center Library
	Commander, U. S. Army Mobility Equipment Research and Development Center, Fort Belvoir, Virginia 22060
1	ATTN: DRDME-MW, Dr. J. W. Bond
2	Technical Documents Center, Building 315
2	Mr. E. York, Matls. Res. Lab., STS-FB-GM
1	Mr. W. McGovern, DRDME-FM
	Commander, U. S. Army Production Equipment Agency, Manufacturing Technology Branch, Rock Island Arsenal, Illinois 61202
1	ATTN: DRXPE, Mr. Ralph Siegel
	Commander, U. S. Army Research and Engineering Directorate, Warren, Michigan 48090
1	ATTN: SMOTA-RCM.1, Mr. Edward Moritz
1	SMOTA-RCM.1, Mr. Donald Phelps
	Commander, Naval Air Engineering Center, Lakehurst, New Jersey 08733
1	ATTN: Technical Library, Code 1115
	Naval Air Development Center, Aero Materials Department, Warminster, Pennsylvania 18974
1	ATTN: J. Viglione

No. of Copies	To
	David Taylor Naval Ship Research and Development Laboratory, Annapolis, Maryland 21402
1	ATTN: Dr. H. P. Chu
	Naval Research Laboratory, Washington, D. C. 20375
1	ATTN: C. D. Beachem, Head, Adv. Matls. Tech. Br. (Code 6310)
1	Dr. J. M. Krafft - Code 8430
1	E. A. Lange
1	Dr. P. P. Puzak
1	R. J. Sanford - Code 8436
1	A. M. Sullivan
1	Mr. R. Rice
	Chief of Naval Research, Arlington, Virginia 22217
1	ATTN: Code 471
1	Dr. Arthur Diness
	Naval Weapons Laboratory, Washington, D. C. 20390
1	ATTN: H. W. Romine, Mail Stop 103
	Director, Structural Mechanics Research, Office of Naval Research, 800 North Quincy Street, Arlington, Virginia 22203
1	ATTN: Dr. N. Perrone
1	Chief, Bureau of Naval Weapons, Department of the Navy, Room 2225, Munitions Building, Washington, D. C.
	Naval Air System Command, Department of the Navy, Washington, D. C. 20360
1	ATTN: Mr. Charles Bersch
1	Ship Research Committee, Maritime Transportation Research Board, National Research Council, 2101 Constitution Avenue, N. W., Washington, D. C. 20418
	Chief, Bureau of Ships, Department of the Navy, Washington, D. C. 20315
1	ATTN: Code 413
	U. S. Army Air Mobility Research and Development Laboratory, Advanced Systems Research Office, Ames Research Center, Moffett Field, California 94035
1	ATTN: F. Immen
1	J Wheatly
	Air Force Materials Laboratory, Wright-Patterson Air Force Base, Ohio 45433
2	ATTN: AFML (MXE), E. Morrissey
1	AFML (LC)
1	AFML (LLP), D. M. Forney, Jr.
1	AFML (LNC), T. J. Reinhart
1	AFFDL (FB), Dr. J. C. Halpin
1	AFML (MBC), Mr. Stanley Schulman
1	AFML (MATB), Mr. George Glenn
1	AFML (LLS), P. Ruh
	Air Force Flight Dynamics Laboratory, Wright-Patterson Air Force Base, Ohio 45433
1	ATTN: AFFDL (FBS), C. Wallace
1	AFFDL (FBE), G. D. Sendeckyj
	National Aeronautics and Space Administration, Washington, D. C. 20546
1	ATTN: Mr. B. G. Achhammer
1	Mr. G. C. Deutsch - Code RW
1	AFSS-AD, Office of Scientific and Technical Information
	National Aeronautics and Space Administration, Marshall Space Flight Center, Huntsville, Alabama 35812
1	ATTN: R. J. Schwinghamer, EH01, Dir, M&P Lab.
1	Mr. W. A. Wilson, EH41, Bldg. 4612
	National Aeronautics and Space Administration, Langley Research Center, Hampton, Virginia 23665
1	ATTN: Mr. H. F. Hardrath, Mail Stop 188M
1	Mr. R. Foye, Mail Stop 188A
	National Aeronautics and Space Administration, Lewis Research Center, 21000 Brookpark Road, Cleveland, Ohio 44135
1	ATTN: Mr. S. S. Manson
1	Dr. J. E. Srawley, Mail Stop 105-1
1	Mr. W. F. Brown, Jr.
1	Mr. M. H. Hirschberg, Head, Fatigue Research Section, Mail Stop 49-1
1	Mr. G. Mervin Ault, Assista ief M&S Division
1	Dr. H. B. Probst, MS 49-1
	Office, Director of Research and Development, Department of the Air Force, The Pentagon, Washington, D. C. 20330
1	ATTN: AFRD-OR, LTC Horas C. Hamlin
1	Major Donald Sponberg
	National Bureau of Standards, U. S. Department of Commerce, Washington, D. C. 20234
1	ATTN Mr. J. A. Bennett
1	Mechanical Properties Data Center, Belfour Stulen Inc., 13917 W. Bay Shore Drive, Traverse City, Michigan 49684

No. of Copies	To
	Defense Materials Service, General Services Administration, Washington, D. C. 20405
1	ATTN: Mr. Clarence A. Fredell, Director, Technical R&D Staff
1	Mr. W. F. Anderson, Atomics International, Canoga Park, California 91303
	Midwest Research Institute, 425 Coker Boulevard, Kansas City, Missouri 64110
1	ATTN: Mr. G. Gross
1	Mr. A. Hurlich, Convair Division, General Dynamics Corp., Mail Zone 630-01, P. O. Box 80847, San Diego, California 92138
1	Mr. J. G. Kaufman, Alcoa Research Laboratories, New Kensington, Pennsylvania 15068
1	Mr. P. N. Randall, TRW Systems Group - 0-1/2210, One Space Park, Redondo Beach, California 90278
1	Mr. W. A. Van der Sluys, Research Center, Babcock and Wilcox, Alliance, Ohio 44601
1	Mr. B. M. Wundt, 2346 Shirl Lane, Schenectady, New York 12309
1	Dr. Raymond Bisplinghoff, Deputy Administrator, National Science Foundation, 1800 G. Street, NW., Washington, D. C. 20550
1	Dr. A. Lovelace, Deputy Assistant Secretary (R&D), Office of Assistant Secretary of the Air Force (Research and Development), Room 4E973, Pentagon, Washington, D. C. 20330
1	Dr. A. R. C. Westwood, RIAS Division of the Martin Company, Baltimore, Maryland
1	Dr. S. Wiederhorn, National Bureau of Standards, Gaithersburgh, Maryland 20760
1	Dr. P. Jorgensen, Stanford Research Institute, Menlo Park, California 94025
1	Mr. M. Allen Magid, Materials Marketing Engineer, Florida R&D Center, Pratt and Whitney Aircraft, P. O. Box 2691, West Palm Beach, Florida 33402
1	Dr. E. A. Steigerwald, TRW Metals Division, P. O. Box 250, Minerva, Ohio 44657
1	Mr. M. J. Manjoin, Westinghouse R&D Center, 1310 Beulah Road, Pittsburgh, Pennsylvania 15235
1	Mr. E. T. Wessel, Westinghouse R&D Center, 1310 Beulah Road, Pittsburgh, Pennsylvania 15235
1	Dr. Alan S. Tetelman, Failure Analysis Associates, 11777 Mississippi Avenue, Suite 4, Los Angeles, California 90025
	Battelle Columbus Laboratories, 505 King Avenue, Columbus, Ohio 43201
1	ATTN: Mr. J. Campbell
1	Dr. G. T. Hahn
1	R. G. Hoagland, Metal Science Group
1	Dr. E. Rybicki
	General Electric Company, Schenectady, New York 12010
1	ATTN: Mr. A. J. Brothers, Materials and Processes Laboratory
	General Electric Company, Schenectady, New York 12309
1	ATTN: Mr. H. F. Bueckner, Large Steam Turbine Generator Department
1	Mr. S. Yukawa, Metallurgy Unit
1	Mr. E. E. Zwicky, Jr.
	General Electric Company, Knolls Atomic Power Laboratory, P. O. Box 1072, Schenectady, New York 12301
1	ATTN: Mr. F. J. Mehringer
1	Mr. L. F. Coffin, Room K41-K1, General Electric Corp., P. O. Box 8, Schenectady, New York 12301
	United States Steel Corporation, Monroeville, Pennsylvania Pennsylvania 15146
1	ATTN: Mr. S. R. Novak
1	Dr. A. K. Shoemaker, Research Laboratory, Mail Stop 78
	Westinghouse Electric Company, Bettis Atomic Power Laboratory, P. O. Box 109, West Mifflin, Pennsylvania 15122
1	ATTN: Mr. M. L. Parrish
	Westinghouse Electric Company, Research Laboratories, Pittsburgh, Pennsylvania 15235
1	ATTN: Dr. R. J. Bratton
	Brown University, Providence, Rhode Island 02912
1	ATTN: Prof. J. R. Rice
1	Prof. W. N. Findley, Division of Engineering, Box D
1	Prof. P. C. Paris
	Carnegie-Mellon University, Department of Mechanical Engineering, Schenley Park, Pittsburgh, Pennsylvania 15213
1	ATTN: Dr. J. L. Swedlow

No. of Copies	To
1	Prof. J. D. Lubahn, Colorado School of Mines, Golden, Colorado 80401
1	Prof. J. Dvorak, Chemical Engineering Department, Duke University, Durham, North Carolina 27706
	George Washington University, School of Engineering and Applied Sciences, Washington, D. C. 20052
1	ATTN: Dr. H. Liebowitz
1	Prof. A. M. Freudenthal
	Lehigh University, Bethlehem, Pennsylvania 18015
1	ATTN: Prof. G. C. Sih
1	Prof. R. Roberts
1	Prof. R. P. Wei
1	Prof. Richard M. Spriggs, Assistant to the President and Professor
1	Prof. D. P. H. Hasselman
	Massachusetts Institute of Technology, Cambridge, Massachusetts 02139
1	ATTN: Prof. B. L. Averbach, Materials Center, 13-5082
1	Prof. F. A. McClintock, Room 1-304
1	Prof. R. M. Pelloux
1	Prof. T. H. H. Pian, Department of Aeronautics and Astronautics
1	Prof. A S. Argon, Room 1-306
1	Prof. R. L. Coble
	Syracuse University, Dept. of Chemical Engineering and Metallurgy, Metallurgy - 409 Link Hall, Syracuse, New York 13210
1	ATTN: Mr. H. W. Liu
1	Dr. V. Weiss, Metallurgical Research Labs., Building D-6
1	Prof. E. R. Parker, Dept. of Materials Science and Engineering, University of California, Berkeley, California 94700
1	Prof. W. Goldsmith, Dept. of Mech. Eng., University of California, Berkeley, California 94720
1	Prof. A. J. McEvily, Metallurgy Dept. U-136, University of Connecticut, Storrs, Connecticut 06268
1	Prof. D. Drucker, Dean of School of Engineering, University of Illinois, Champaign, Illinois 61820
	University of Illinois, Urbana, Illinois 61801
1	ATTN: Prof. H. T. Corten, Dept. of Theoretical and Applied Mechanics, 212 Talbot Laboratory
1	Prof. T. J. Dolan, Dept. of Theoretical and Applied Mech.
1	Prof. J. Morrow, 321 Talbot Laboratory
1	Mr. G. M. Sinclair, Dept of Theoretical and Applied Mech.
1	Prof. R. I. Stephens, Materials Engineering Div., University of Iowa, Iowa City, Iowa 52242
1	Prof. D. K. Felbeck, Dept. of Mechanical Engineering, University of Michigan, 2046 East Engineering, Ann Arbor, Michigan 48109

No. of Copies	To
1	Dr. N. L. Williams, Dean of Engineering, 240 Benedum Hall, University of Pittsburgh, Pittsburgh, Pennsylvania 15261
1	Prof. A. Kobayashi, Dept. of Mechanical Engineering, Fu-10, University of Washington, Seattle, Washington 98195
	Albany Metallurgy Research Center, Albany, Oregon 97321
1	ATTN: Mr. R. R. Wells, Research Director
	Ford Motor Company, Turbine Research Department, 20000 Rotunda Drive, Dearborn, Michigan 48121
1	ATTN: Mr. A. F. McLean
	IIT Research Institute, 10 West 35 Street, Chicago, Illinois 60616
1	ATTN: Mr. S. Bortz, Ceramics Research
	United Aircraft Research Laboratories, East Hartford, Connecticut 06108
1	ATTN: Dr. Michael DeCrescenti
	State University of New York, College of Ceramics at Alfred University, Alfred, New York 14802
1	ATTN: Mr. Satyavan Shukla, Assistant Librarian
	SKF Industries, Inc., Engineering and Research Center, 1100 1st Avenue, King of Prussia, Pennsylvania 19406
1	ATTN: Harish Dalal
	Deposits and Composites, Inc., 1821 Michael Drive, Reston, Virginia 22090
1	ATTN: Mr. Richard E. Engdahl, President
	AiResearch Mfg. Co. of Arizona, 402 South 36th Street, Phoenix, Arizona 85034
1	ATTN: Chief, Materials Engineering Department, Dept. 93-39M
	Monsanto Research Corp., Dayton Laboratory, 1515 Nicholas Road, Dayton, Ohio 45407
1	ATTN: Mr. Richard J. Janowiecki, Research Group Leader
	Norton Company, 1 New Bond Street, Worcester, Massachusetts 01606
1	ATTN: Dr. H. R. Baumgartner
	Federal Mogul Corporation, Bearing Group Research, 3980 Research Park Drive, Ann Arbor, Michigan 48104
1	ATTN: Mr. P. E. Cowley
	Energy Research and Development Administration, Division of Transportation, Highway Vehicles Systems Brarch, 20 Massachusetts Avenue, NW, Washington, D. C.
1	ATTN: Mr. G. Thur
1	Mr. R. Schulz
	State University of New York at Stony Brook, Stony Brook, New York 11790
1	ATTN: Prof. Fu-Pen Chaing, Dept. of Mechanics
	Director, Army Materials and Mechanics Research Center, Watertown, Massachusetts 02172
2	ATTN: DRXMR-PL
1	DRXMR-AG
1	Author

Army Materials and Mechanics Research Center,
Watertown, Massachusetts 02172
RESIDUAL STRESSES IN AN ANISOTROPIC THICK-HOLLOW CYLINDER OF CHEMICALLY VAPOR-DEPOSITED MATERIAL DUE TO UNIFORM COOL-DOWN - Francis I. Baratta

Technical Report AMMRC TR 77-2., October 1977, 26 pp - illus-table, D/A Project 1T161101A91A, AMCMS Code 611101.91A0011

AD________________

UNCLASSIFIED
UNLIMITED DISTRIBUTION

Key Words

Residual stress
Vapor deposition
Anisotropy

Residual stresses are derived for a transversely anisotropic thick hollow cylinder which has been chemically vapor deposited at an elevated temperature. Such stresses arise because of the differential rates of contraction in the radial and tangential directions and the anisotropic elastic constants. Residual stress distributions for cylinders with a wall ratio (outer to inner radius) of 1.30 of pyrolytic graphite and pyrolytic silicon carbide (α-SiC) are presented as a function of the radius to inner radius. The effect of the variation of the elastic anisotropy on the tangential stress at the inner and outer radii is presented as a function of the wall ratio. Finally, the tangential and axial stresses at the inner and outer radii and the maximum radial stress of chemically vapor-deposited α-SiC are presented as a function of the wall ratio.

Army Materials and Mechanics Research Center,
Watertown, Massachusetts 02172
RESIDUAL STRESSES IN AN ANISOTROPIC THICK-HOLLOW CYLINDER OF CHEMICALLY VAPOR-DEPOSITED MATERIAL DUE TO UNIFORM COOL-DOWN - Francis I. Baratta

Technical Report AMMRC TR 77-2., October 1977, 26 pp - illus-table, D/A Project 1T161101A91A, AMCMS Code 611101.91A0011

AD________________

UNCLASSIFIED
UNLIMITED DISTRIBUTION

Key Words

Residual stress
Vapor deposition
Anisotropy

Residual stresses are derived for a transversely anisotropic thick hollow cylinder which has been chemically vapor deposited at an elevated temperature. Such stresses arise because of the differential rates of contraction in the radial and tangential directions and the anisotropic elastic constants. Residual stress distributions for cylinders with a wall ratio (outer to inner radius) of 1.30 of pyrolytic graphite and pyrolytic silicon carbide (α-SiC) are presented as a function of the radius to inner radius. The effect of the variation of the elastic anisotropy on the tangential stress at the inner and outer radii is presented as a function of the wall ratio. Finally, the tangential and axial stresses at the inner and outer radii and the maximum radial stress of chemically vapor-deposited α-SiC are presented as a function of the wall ratio.

Army Materials and Mechanics Research Center,
Watertown, Massachusetts 02172
RESIDUAL STRESSES IN AN ANISOTROPIC THICK-HOLLOW CYLINDER OF CHEMICALLY VAPOR-DEPOSITED MATERIAL DUE TO UNIFORM COOL-DOWN - Francis I. Baratta

Technical Report AMMRC TR 77-2., October 1977, 26 pp - illus-table, D/A Project 1T161101A91A, AMCMS Code 611101.91A0011

AD________________

UNCLASSIFIED
UNLIMITED DISTRIBUTION

Key Words

Residual stress
Vapor deposition
Anisotropy

Residual stresses are derived for a transversely anisotropic thick hollow cylinder which has been chemically vapor deposited at an elevated temperature. Such stresses arise because of the differential rates of contraction in the radial and tangential directions and the anisotropic elastic constants. Residual stress distributions for cylinders with a wall ratio (outer to inner radius) of 1.30 of pyrolytic graphite and pyrolytic silicon carbide (α-SiC) are presented as a function of the radius to inner radius. The effect of the variation of the elastic anisotropy on the tangential stress at the inner and outer radii is presented as a function of the wall ratio. Finally, the tangential and axial stresses at the inner and outer radii and the maximum radial stress of chemically vapor-deposited α-SiC are presented as a function of the wall ratio.

Army Materials and Mechanics Research Center,
Watertown, Massachusetts 02172
RESIDUAL STRESSES IN AN ANISOTROPIC THICK-HOLLOW CYLINDER OF CHEMICALLY VAPOR-DEPOSITED MATERIAL DUE TO UNIFORM COOL-DOWN - Francis I. Baratta

Technical Report AMMRC TR 77-2., October 1977, 26 pp - illus-table, D/A Project 1T161101A91A, AMCMS Code 611101.91A0011

AD________________

UNCLASSIFIED
UNLIMITED DISTRIBUTION

Key Words

Residual stress
Vapor deposition
Anisotropy

Residual stresses are derived for a transversely anisotropic thick hollow cylinder which has been chemically vapor deposited at an elevated temperature. Such stresses arise because of the differential rates of contraction in the radial and tangential directions and the anisotropic elastic constants. Residual stress distributions for cylinders with a wall ratio (outer to inner radius) of 1.30 of pyrolytic graphite and pyrolytic silicon carbide (α-SiC) are presented as a function of the radius to inner radius. The effect of the variation of the elastic anisotropy on the tangential stress at the inner and outer radii is presented as a function of the wall ratio. Finally, the tangential and axial stresses at the inner and outer radii and the maximum radial stress of chemically vapor-deposited α-SiC are presented as a function of the wall ratio.